2021 IEEE/RSJ International Conference on Intelligent Robots and Systems (IROS)
September 27 - October 1, 2021. Prague, Czech Republic

A Motion decoupled Aerial Robotic Manipulator for Better Inspection

Rui Peng, Xianda Chen and Peng Lu

2021 IEEE/RSJ International Conference on Intelligent Robots and Systems (IROS) | 978-1-6654-1714-3/21/$31.00 ©2021 IEEE | DOI: 10.1109/IROS51168.2021.9636765

***Abstract*—For conventional aerial manipulators, the robotic arm is rigidly attached to the quadrotor. Consequently, the maneuver of the quadrotor will affect the motion of the robotic arm when it is used for tasks such as inspection. In this paper, we propose a novel aerial manipulator with a self-locking gimbal system which can switch between motion coupled and decoupled mode. Furthermore, a dynamic gravity compensation mechanism is designed, where the location of the battery and the number of teeth are optimized to minimize the weight imbalance of the robotic arm during its motions. To the best of the authors' knowledge, this is the first aerial manipulator with a motion-decoupled mechanism. Experimental results demonstrate that the proposed manipulator design can significantly improve the performance of the manipulator for general inspection tasks.**

I. Introduction

Unmanned aerial vehicles (UAV) equipped with a robotic arm are endowed with capabilities of physical interaction with surrounding environments, which enriches their real-life applications explosively, such as height-working or inspection, aerial grasping, military use, human rescue and aerial manipulation [1], [2].

From the perspective of mechanical structure, previous researches on aerial manipulators mainly focus on designing a traditional humanoid robotic arm with certain amount of links and joints. For example, a two degrees of freedom (DOF) manipulator is deployed in a quadrotor with an adaptive sliding controller to perform object picking and delivering tasks [3]. With visual trajectory tracking, a light-weight aerial manipulator is developed to implement autonomous grasping control [4]. Based on an eight rotors vehicle with a large payload capacity, a 7-DOF arm is designed for outdoor operation [5]. To open and close a drawer in unknown conditions, a quadrotor combined with a robotic arm [6] is proposed to tackle the uncertainties of the drawer's mechanism, with strategies exploiting the velocity of the end-effector. Attached to the top of a multirotor, an aerial robotic multi-link arm [7] has strong capabilities for building inspection, such as taking measurements from the underside of a bridge. A dual-arm aerial manipulator [8] is used to conduct valve turning, with force feedback on interaction between the manipulator and the environment. Relying on a variable parameter integral backstepping controller, an aerial robot [9] is implemented for assembly missions.

In addition to humanoid manipulators, other researches have proposed specific designs aimed at specialized tasks [10] such as door pushing [11], bird-inspired perching and grasping [12]. To achieve an extensive reachable space, a redundant aerial manipulator system is derived with coupled dynamics of the aerial vehicle and the manipulator [13]. Later, a novel configuration of an aerial manipulator [14] is proposed to implement perching function, knob-twisting function, and door-opening function. To access into confined spaces, an origami-inspired, extensible aerial robotic arm is designed, with a stiffening mechanism using an origami principle of perpendicular folding [15]. To address the high risks in large-scale on-site infrastructure inspection, a compact aerial manipulator [16] with one single DOF is developed for placing and retrieving sensors in the environment.

Compared with regular UAVs, an aerial manipulator system suffers frequently from weight-imbalance and motion inertia during flights [17] This can cause an increased time-latency for the UAV's attitude response and impair its stability when performing aerial manipulation tasks. Consequently, the UAV must rely on a sophisticated and well-tuned flight controller to maintain its robustness and agility, raising the challenges in algorithm development and further validations [18]. From the perspective of mechanical design, this paper is intend to release the demand on the flight controller and reduce the disturbance caused by the motion of the robotic arm [19].

In this paper, a motor-controlled self-locking gimbal is proposed to switch between the coupled and decoupled status between the UAV and the manipulator which is based on the four-bar linkage mechanism. When the gimbal is unlocked, the robotic arm's attitude is decoupled from the motion of the UAV, making it less effected by the inertia of the arm during flight maneuver. On the other hand, the gimbal is locked when the UAV is hovering at the designated position and the inspection task is being carried out. Additionally, a gravity-compensation system inspired by [20] is designed to optimize the aerial manipulator's gravity distribution and neutralize the weight imbalance during the manipulator's movement.

The main contributions of this paper are summarized as follows:

1) A self-locking gimbal controlling two DOF (roll and pitch) is designed to switch the coupled and decoupled status of the aerial manipulator.
2) A dynamic gravity compensation mechanism is designed to minimize the change of gravity of the robotic arm during its motions.
3) Experiments results demonstrate that the self-locking gimbal and the dynamic gravity compensation system are effective in reducing the flight disturbance.

The authors are with the Department of Mechanical Engineering, The University of Hong Kong. (Email: lupeng@hku.hk). The attachment video link of this work: https://www.youtube.com/watch?v=a056onq0OPM

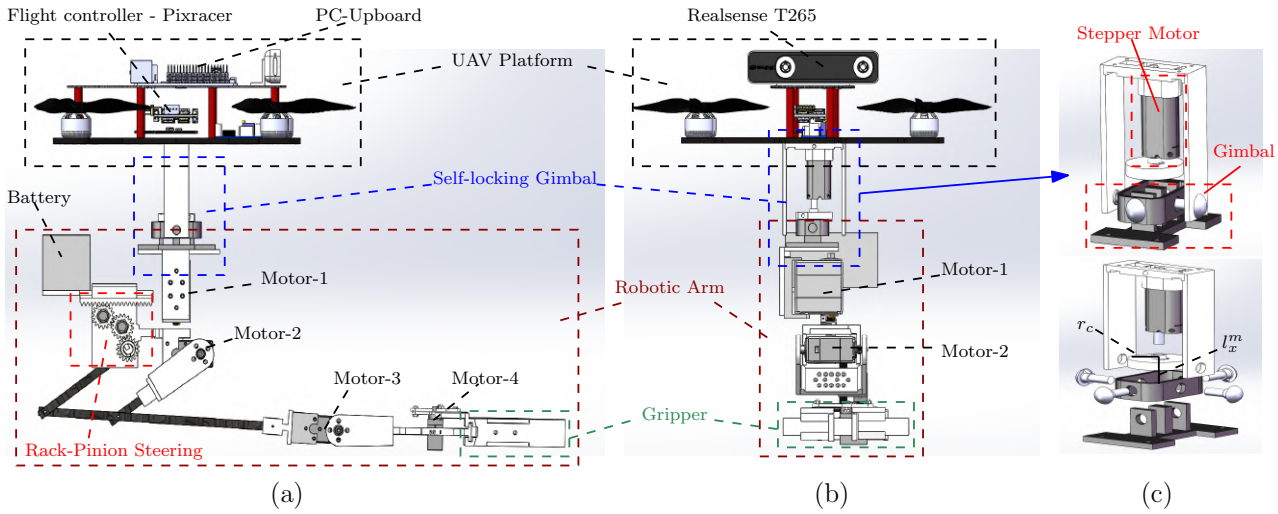

Fig. 1. The detailed system architecture of the proposed aerial robotic manipulator. (a) Side view. (b) Front view. (c) Structure of the self-locking gimbal.

II. Aerial Manipulator Mechanism

A. System Overview

The architecture of the proposed aerial manipulation system is shown in Fig. 1, which consists of three parts: a UAV platform, a self-locking gimbal and a four-bar linkage robotic arm. The system is assembled strictly so that its initial center of gravity is located at the center planar of the drone. An electronic embedded system is also deployed to implement motion control.

B. Self-locking Gimbal

The gimbal system is designed to switch the mechanism between decoupled mode and coupled mode, indicating the attitude of the drone and the robotic arm. In the decoupled mode, the motion of the UAV can not affect the attitude of the robot arm, so that the arm will not introduce much disturbance to the drone. The drone and the arm will keep the same attitude in the coupled mode, which is necessary for manipulation. It contributes to state estimation and kinematics analysis.

The proposed gimbal rotates along two axes as shown in Fig. 1, giving the freedom of roll ${}^G\phi$ and pitch ${}^G\theta$ (except yaw) to the downward robotic arm. A linear stepper motor is employed to adjust the attitude of the gimbal, which is the predominant innovation of our proposal. The stepper motor is installed above the pivoted part, with a circle hard piece attached on its moving tip. The tip moves perpendicular to the x-y plane and the circle piece works parallel to the plane. Thus, the attitude of the gimbal are restricted by the stepper motor, which can be modeled as:

$$ {}^G\phi, {}^G\theta \in (0, \arctan(\frac{l_x^m}{r_c})) \tag{1}$$

where r_c is radius of the circle piece, and l_x^m is distance between the circle piece and the gimbal plane.

A decoupling degree can be established according to Eq.(1), depending on the variable l_x^m. When the UAV maneuvers aggressively, the UAV is still affected by the downward robotic arm, with limited range of the gimbal by a small constant l_x^m. But when the UAV only executes normal moves, it takes redundant time to switch to the coupled mode, with a large constant l_x^m. Based on the discussion above, to improve the performance of the decoupled mode during the UAV flights, real-time attitude change of the UAV should be considered. With attitude estimation from the UAV's flight controller, we denote the pitch and roll of the UAV as ${}^U\phi$ and ${}^U\theta$.

where α is a constant parameter larger than 1, which ensures that maximum of the gimbal angle is larger than the aligned realtime euler angle of the UAV. Also, l_x^m is proportional to the euler angle.

The aim of the decoupled mode is to reduce disturbance from the robotic arm part for better stability of the UAV platform. According to the equation 2, attitude change of the UAV during flights does not introduce rotation inertia, which is associated with the arm. The coupled mode is activated when l_x^m equals to 0, and the circle piece physically contacts the gimbal part with no gap. Due to the contact, motion of the gimbal structure is therefore restricted. The coupled feature for the aerial manipulator system is discussed in subsequent paragraphs.

The coupled mode ensures a unified system including the UAV and the robotic arm, with a relative static contact frame. The gimbal part is "locked" by the stepper motor ($l_x^m = 0$). However, to perfectly implement the locking function, one crucial problem needs to be addressed. The problem is the locking performance, which is evaluated by the gap between the circle piece and the gimbal plane. Evidently, the larger push-pressure of the piece, the better the locking performance is, with little gap. To model the push-pressure, push-force of the stepper motor should be taken into consideration. Also, denoting the contact area of the gap as S_c and the push-force as F_m, the push-pressure

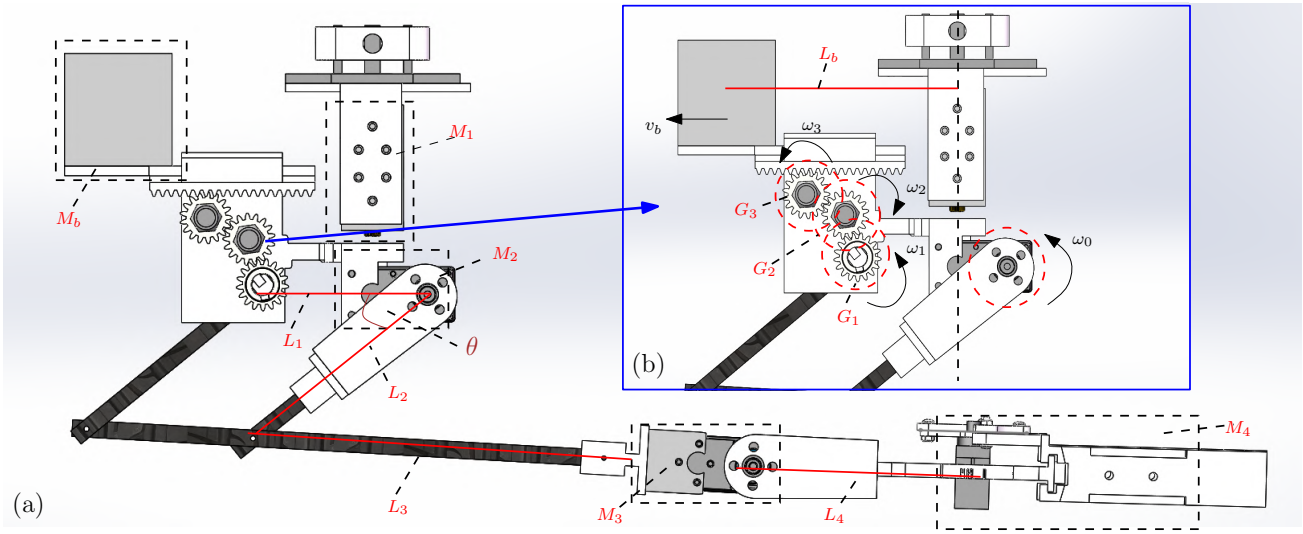

Fig. 2. Structural configuration of the four-bar linkage mechanism based robotic arm (a) and the gravity compensation system (b).

P_g on the robotic arm is given by:

$$P_g = \frac{F_m}{S_c} \tag{2}$$

where S_c is a constant value according to mechanical design of the gimbal part. On the other hand, potential motion of the robotic arm generates the inverse pressure P'_g to the gimbal part. Taking mass and torque of the designed arm into account, P_g is proved to be larger than P'_g in experiments. Thus, the coupled mode provides constant transformation between marked coordinates for the aerial manipulation system.

C. Four-bar linkage Robotic Arm

The four-bar linkage mechanism is a lightweight and concise movable closed-chain linkage mechanism, comprised of four links that are connected in a loop with four revolute joints. Generally, the four-bar linkage mechanism can be used to realize long-stroke motions, even with only one servo motor on the joint. Based on this inspiration, a four-bar linkage mechanism based robotic arm is designed with the capability to reach a large end-effector motion range. The detailed mechanical design of the robotic arm is shown in Fig. 2.

D. Motion decoupled Function Validation

To model the rigid robotic arm, the Denavit-Hartenberg (D-H) parameters are used to formulate the body kinematics. Then, the frame reference of the end-effector can be obtained by applying forward kinematics. On the other hand, the end-effector is controlled to reach the solved targeted pose, according to the formulated inverse kinematics. Fig. 2 shows the frame coordinates and the D-H parameters of the arm.

The robotic arm has three degrees of freedom. Based on the four-bar linkage design, the forward motion of the arm can be driven by only one servo motor and the end-effector is able to reach out of the UAV plane. Through using lightweight materials to realize the design, the overall weight of the proposed aerial manipulator with the UAV platform included is limited in less than 1kg. When using the 2204 motors, the platform can provide in total more than 2.2 kg lift and can lift a maximum payload of 1.2 kg when performing inspection tasks.

E. Dynamic Gravity Compensation Mechanism

When the manipulator is in operation, the system is switched into the coupled mode. Under this circumstance, motion of the robotic arm introduces rotation torque to the UAV platform. To maintain the stability, the UAV is required to provide extra torque to neutralize the torque of the robotic arm. Conventionally, previous research focus on design of UAV controller, to handle the issue. But it involves many factors, such as motor, UAV prototype, computational device and so on. Therefore, from the perspective of mechanical design, we propose a dynamic gravity compensation mechanism to minimize the torque adjustment of the UAV, shown in Fig. 2.

To compensate for the positive torque of the arm's motion, there must exist an equal negative torque from the other side. We utilize the battery as the dynamic weight source, and it is linearly movable. To implement it, the battery is mounted on a rack-and-pinion structure. The structure could transform rotation moves to linear moves. Based on the four-bar linkage, one of the joints is taken as the rotation origin of the structure. Since each joint of the linkage is associated, the motion of the robotic arm will generate an inverse motion for the battery.

The aim of this compensation design is to make the gravity center as close as possible to the central line of the aerial system. By doing this, when the robotic arm is moving, it will not introduce additional disturbance to the quadrotor.

We use the center of the quadrotor as the origin. Given that motor 1 and 2 are located the center of the quadrotor,

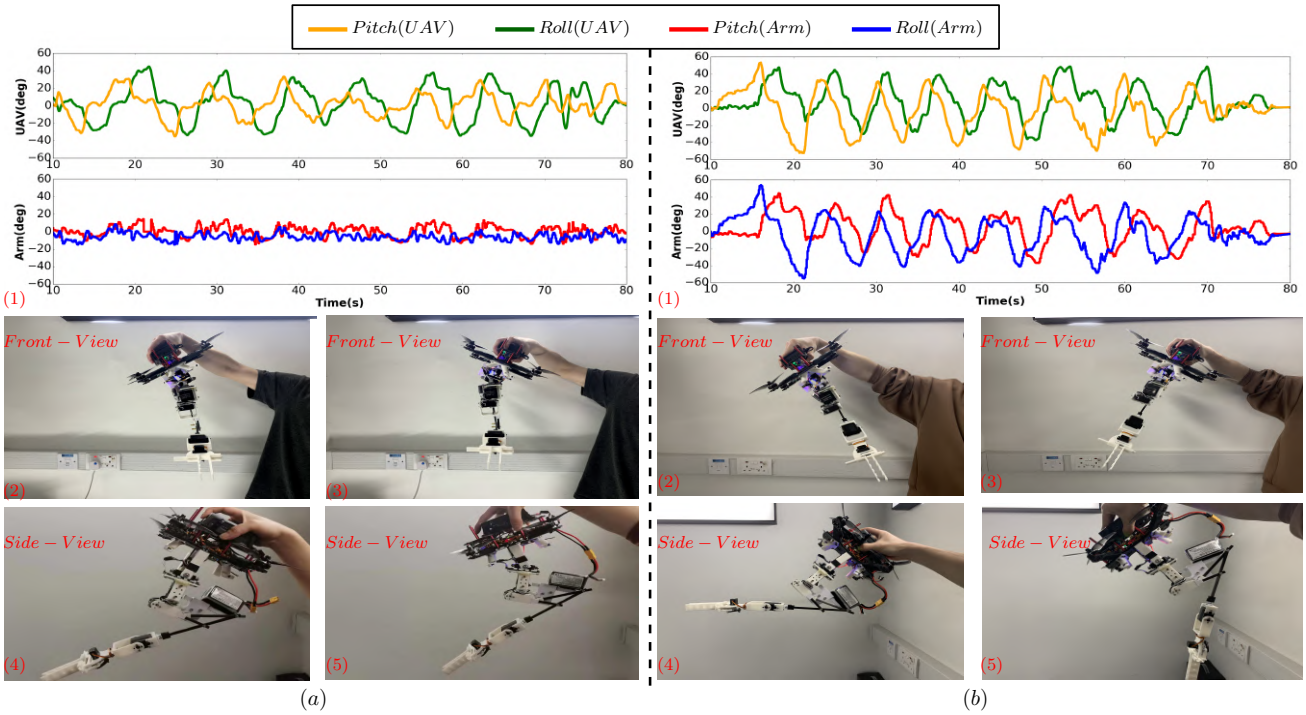

Fig. 3. Decoupled function validation in hand-manipulation. (a) Decoupled mode. (b) Coupled mode. From front view and side view, snapshots:(a,b-2,3,4,5) show different extreme attitudes of the UAV. (a-1) and (b-1) present attitude variation of the UAV and the robotic arm during 80s hand-manipulation.

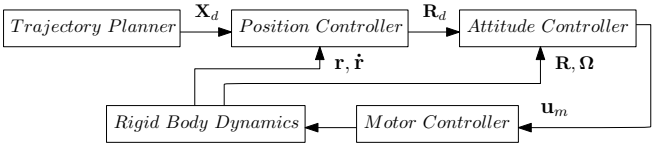

Fig. 4. Control framework of the aerial manipulator.

the real-time location of the gravity center of the robotic arm including the compensation system, is given as:

$$M\,{}^{g}x_o = -M_b L_b + (x_3 - L_2\cos\theta)M_3 + (x_4 - L_2\cos\theta)M_4 \tag{3}$$

with

$$L_b = L_0 + \theta_3 r_3 \tag{4}$$

$$x_3 = L_3 - L_2\sin\theta \tag{5}$$

$$x_4 = L_3 + L_4 - L_2\sin\theta \tag{6}$$

where L_b is the location of the battery, L_0 denotes its initial position, θ_3 and r_3 denote the rotational angle and radius of the topmost gear respectively. M_b, M_3 and M_4 are mass of the battery, servo motor-3 and servo motor-4 respectively. $M = M_1 + M_2 + M_3 + M_4 + M_b$ is the total mass of the manipulator. L_1, L_2, L_3, L_4 are the arm lengths of the four link and M_1, M_2, M_3, M_4 are the mass of the four motors, respectively. Detailed illustration is shown in Fig. 2.

Let n_3 denote the number of teeth of the topmost gear, our goal is to minimize the following cost function:

$$\underset{L_0, n_3}{argmin} \int_0^{\frac{5}{6}\pi} {}^{g}x_o^2 d\theta \tag{7}$$

As seen in Eq. (3), ${}^{g}x_o$ is the function of L_0, n_3 and θ. We use numerical method to find the optimal L_0 and n_3 that minimize the cost function in Eq. (7). We will validate the effectiveness of the obtained parameter in the following section.

III. Experimental Results

A. Control Framework

The control problem of the aerial manipulator is solved by the trajectory tracking controller, position controller and attitude controller. The controllers build a complete control system for the UAV, shown as Fig. 4.

B. Gravity Compensation Validation

For aerial manipulation tasks, a specific 3D trajectory is assumed already planned in advance for the manipulator. The trajectory is formed by a sequence of positions, denoted by an $n \times 3$ matrix $X_T = \{X_1, X_2, ..., X_n\}$. For each position, there is a corresponding yaw angle ψ for the UAM. Thus, a trajectory planner is established for the tracking controller as:

$$T_p^{des} = \begin{bmatrix} X_T(t) \\ \psi_T(t) \end{bmatrix} \tag{8}$$

Given a set-point, the position controller computes errors between its current position and the point, to generate desired Euler angles, denoted as $[\theta_i^{des}, \phi_i^{des}, \psi_i^{des}]$. Then, a

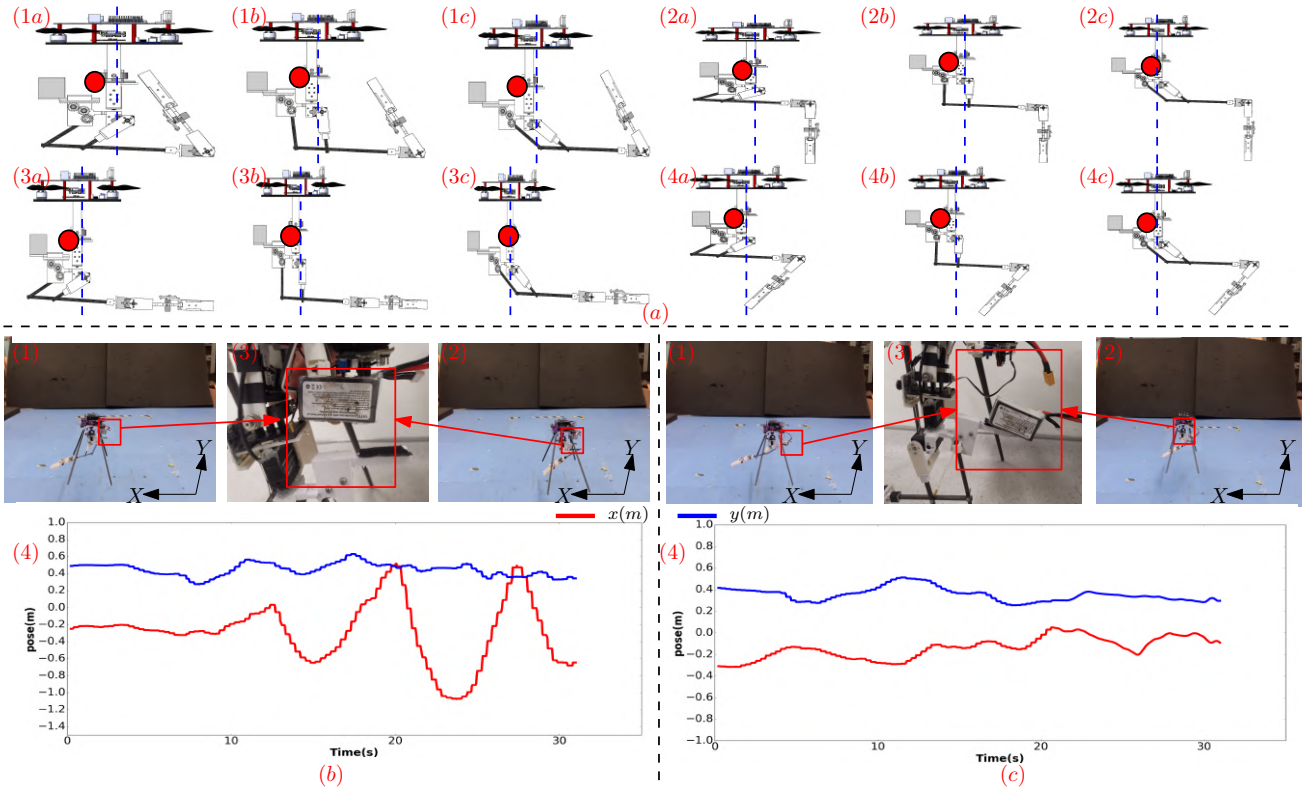

Fig. 5. Validation of the gravity compensation system. (a) Gravity modeling with various states of the robotic arm in Solidworks software, with red points (gravity center point) and blue dashed lines (center line). (b) Actual hovering flights in the coupled mode with two contrary states of the battery. (b-4) presents the localization pose (x, y) with respect to time (0-30s). (c) shows the correct configuration of the battery on the compensation system, and other information is same as the (b).

PD (proportional and derivative) attitude controller is used to track the desired Euler angles in SO(3). Motor control thrust is given by:

$$\mathbf{M}_T = \begin{bmatrix} k_{p,\theta}(\theta^{des} - \theta^c) + k_{d,\theta}(\dot{\theta}^{des} - \dot{\theta}^c) \\ k_{p,\phi}(\phi^{des} - \phi^c) + k_{d,\phi}(\dot{\phi}^{des} - \dot{\phi}^c) \\ k_{p,\psi}(\psi^{des} - \psi^c) + k_{d,\psi}(\dot{\psi}^{des} - \dot{\psi}^c) \end{bmatrix} \quad (9)$$

For control of the robotic arm, the inverse kinematics solves the corresponding rotating angles of joint-motors, according to a point in cartesian space. The motors drive the robotic arm to make the end-effector reach the targeted point.

To validate the decoupled function of the proposed system, two IMU (Inertia Measurement Unit) sensors are implemented to detect the attitudes of the UAV and the robotic arm. An IMU is embedded in the flight controller board, and the other one is mounted on the level-plane of the arm. When the decoupled mode is activated, the UAV and the robotic arm are two independent parts. Reflected on the IMU readings, the altitude of the robotic arm should be unaffected by the movement of the UAV theoretically. On the other hand, the UAV is rigidly linked with the arm in the coupled mode, which means that their attitudes should be consistent. To demonstrate these decoupled and coupled features, the results of a hand-manipulation experiment for the aerial platform are presented. During the manipulation, the IMUs' real-time measurement readings under the two modes are recorded respectively.

In the experiment, the IMU sensors can measure and present the attitude-difference between the UAV part and the robotic arm part during the motion. As shown in Fig. 3, the comparison results fully validate the effectiveness of the decoupled function. Based on this function, an improved flight performance of the aerial manipulator is achieved.

The gravity of the robotic arm affects the motion performance of the proposed system. The gravity-compensation system is designed to reduce gravity shifts due to the motion of the robotic arm. Then, the stability of the UAV is improved. To validate the performance of the compensation system, one key issue is to detect the gravity position locating on the system. It is quite complicated to detect the gravity position accurately. Therefore, we design a hovering flight experiment with the same flight controller under two states: the battery is attached to the UAV platform fixedly and the battery is mounted on the compensation system correctly. The aerial manipulator activates the coupled mode, with the robotic arm moving. By comparing the pose (x, y) shift of the two states during the flight, the gravity compensation system is ensured to reduce interference of the robotic arm for the UAV platform. The battery configuration in actual flights and pose results are depicted in Fig. 5, where

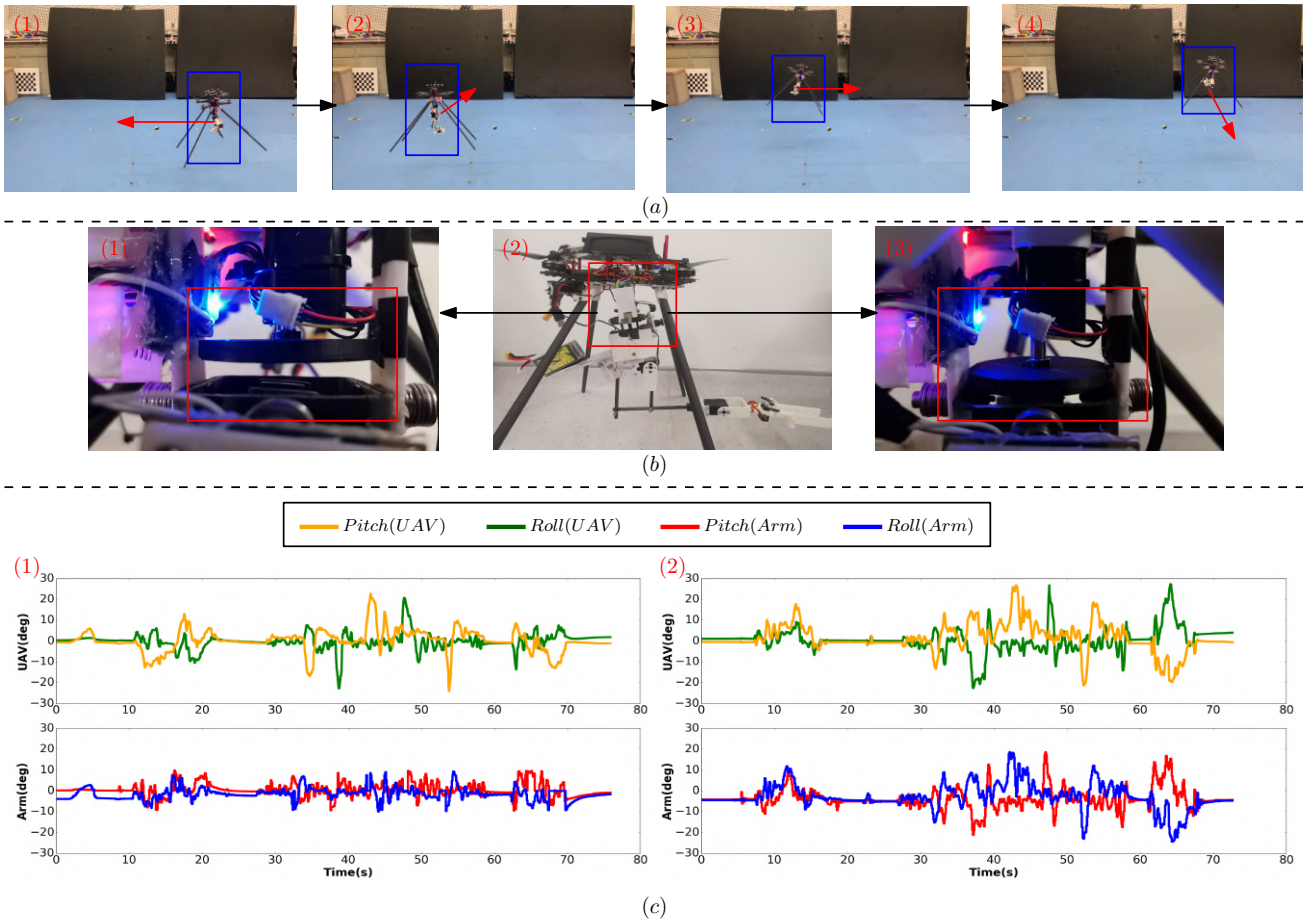

Fig. 6. Decoupled function validation in an actual flight following an inspection path. (a) The aerial manipulator is flying in a square path, with red arrows pointing to the next path point. (b) Mechanical presentation of the decoupled (b-1) and coupled (b-3) mode. (c) Comparison of IMU measurement results between the decoupled (c-1) and coupled (c-2) mode in a 70s flight. Inspection flight. (d) The robotic arm is equipped with a mono camera, which is used to capture inspection images of the object (boxes). (e) First startup point of the coupled mode (1) and the decoupled mode (2) with red arrows pointing to the moving direction. (f) Second startup point of the coupled mode (3) and the decoupled mode (4) with the same information as the (e).

we simulate the gravity center of the mechanical structure in Solidworks.

C. Inspection Maneuvers

The proposed motion decoupled and dynamic gravity compensation is designed for better inspection. For example, bridge and building inspection require advanced technologies to improve efficiency and lower down human-danger. Based on our aerial system, the inspection device could be installed on the decoupled robotic arm. During the inspection, the attitude of the device is not affected by the motion of the UAV under the decoupled mode. Firstly, We design a square-flight inspection experiment. Under the two motion modes (decoupled and coupled modes), the system follows a predefined square path and record IMU measurement data of both the UAV and the robotic arm. The actual configuration of the decoupled and coupled mode and IMU comparison results are depicted in Fig. 6.

We equip the robotic arm with a mono camera shown in Fig. 7 (a), which captures images during inspection flights. Also, a flight path is designed for the inspection object. We select two consecutive frames when the system is moving, shown in Fig. 7 (b, c). When the coupled mode is activated, the frame flow of the camera is evidently shaking due to the physical consistency with the UAV. Meanwhile, the frame flow is more stable during the decoupled mode. By comparing the image-difference under both the decoupled and coupled modes, the inspection function of the proposed system is validated.

IV. Conclusion

In this paper, a motion decoupled aerial manipulator system is proposed based on a self-locking gimbal and a four-bar linkage based robotic arm. The concept of coupled and decoupled status switching in aerial manipulator design is to our best knowledge firstly presented and validated. When the manipulator is decoupled to a UAV, the disturbance caused by the robotic arm during flight is reduced and the design demand on the UAV flight controller is alleviated. Based on the four-bar linkage mechanism, a forward kinematics modelling for the robotic arm is established and a gravity compensation mechanism is proposed to neutralize

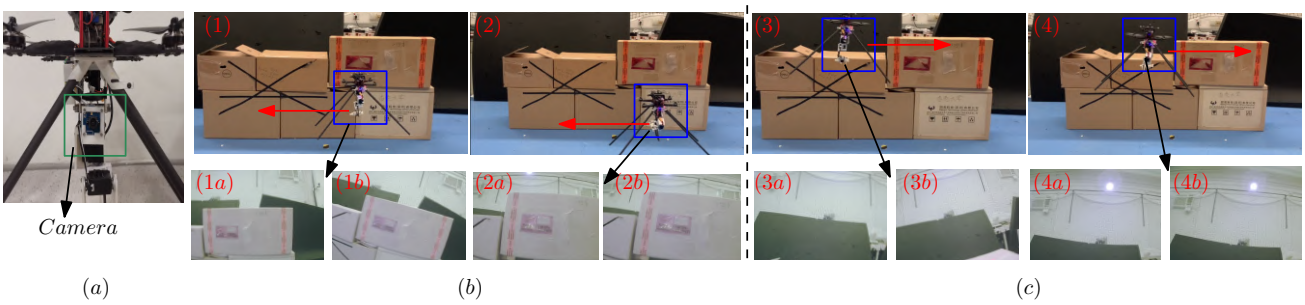

Fig. 7. Inspection flight. (a) The robotic arm is equipped with a mono camera, which is used to capture inspection images of the object (boxes). (b) First startup point of the coupled mode (1) and the decoupled mode (2) with red arrows pointing to the moving direction. (c) Second startup point of the coupled mode (3) and the decoupled mode (4) with the same information as the (b). (1a-1b), (3a-3b) show two consecutive frames when the system is moving under the coupled mode, which cause issue of large rotation. (2a-2b), (4a-4b) in the decoupled mode will not introduce much interference to the inspection images.

the weight imbalance during the manipulator's movement. Experiments have demonstrated and validated the favourable performance of the aerial manipulator system and its efficiency is improved compared with conventional designs.

REFERENCES

[1] S. Cocuzza, E. Rossetto, G. Rosati, and A. Doria, "Decoupled dynamic model of an aerial manipulator."

[2] P. J. Sanchez-Cuevas, A. Gonzalez-Morgado, N. Cortes, D. B. Gayango, A. E. Jimenez-Cano, A. Ollero, and G. Heredia, "Fully-actuated aerial manipulator for infrastructure contact inspection: Design, modeling, localization, and control," *Sensors*, vol. 20, no. 17, p. 4708, 2020.

[3] S. Kim, S. Choi, and H. J. Kim, "Aerial manipulation using a quadrotor with a two dof robotic arm," in *2013 IEEE/RSJ International Conference on Intelligent Robots and Systems*. IEEE, 2013, pp. 4990–4995.

[4] H. Chen, F. Quan, L. Fang, and S. Zhang, "Aerial grasping with a lightweight manipulator based on multi-objective optimization and visual compensation," *Sensors*, vol. 19, no. 19, p. 4253, 2019.

[5] G. Heredia, A. Jimenez-Cano, I. Sanchez, D. Llorente, V. Vega, J. Braga, J. Acosta, and A. Ollero, "Control of a multirotor outdoor aerial manipulator," in *2014 IEEE/RSJ international conference on intelligent robots and systems*. IEEE, 2014, pp. 3417–3422.

[6] S. Kim, H. Seo, and H. J. Kim, "Operating an unknown drawer using an aerial manipulator," in *2015 IEEE International Conference on Robotics and Automation (ICRA)*. IEEE, 2015, pp. 5503–5508.

[7] A. Jimenez-Cano, J. Braga, G. Heredia, and A. Ollero, "Aerial manipulator for structure inspection by contact from the underside," in *2015 IEEE/RSJ international conference on intelligent robots and systems (IROS)*. IEEE, 2015, pp. 1879–1884.

[8] C. Korpela, M. Orsag, and P. Oh, "Towards valve turning using a dual-arm aerial manipulator," in *2014 IEEE/RSJ International Conference on Intelligent Robots and Systems*. IEEE, 2014, pp. 3411–3416.

[9] H. Tsukagoshi, M. Watanabe, T. Hamada, D. Ashlih, and R. Iizuka, "Aerial manipulator with perching and door-opening capability," in *2015 IEEE International Conference on Robotics and Automation (ICRA)*. IEEE, 2015, pp. 4663–4668.

[12] A. E. Jimenez-Cano, J. Martin, G. Heredia, A. Ollero, and R. Cano, "Control of an aerial robot with multi-link arm for assembly tasks," in *2013 IEEE International Conference on Robotics and Automation*. IEEE, 2013, pp. 4916–4921.

[10] S.-J. Kim, D.-Y. Lee, G.-P. Jung, and K.-J. Cho, "An origami-inspired, self-locking robotic arm that can be folded flat," *Science Robotics*, vol. 3, no. 16, 2018.

[11] A. Nikou, G. C. Gavridis, and K. J. Kyriakopoulos, "Mechanical design, modelling and control of a novel aerial manipulator," in *2015 IEEE International Conference on Robotics and Automation (ICRA)*. IEEE, 2015, pp. 4698–4703.

[13] D. Mellinger, Q. Lindsey, M. Shomin, and V. Kumar, "Design, modeling, estimation and control for aerial grasping and manipulation," in *2011 IEEE/RSJ International Conference on Intelligent Robots and Systems*. IEEE, 2011, pp. 2668–2673.

[14] C. E. Doyle, J. J. Bird, T. A. Isom, C. J. Johnson, J. C. Kallman, J. A. Simpson, R. J. King, J. J. Abbott, and M. A. Minor, "Avian-inspired passive perching mechanism for robotic rotorcraft," in *2011 IEEE/RSJ international conference on intelligent robots and systems*. IEEE, 2011, pp. 4975–4980.

[15] M. Tognon, H. A. T. Chávez, E. Gasparin, Q. Sablé, D. Bicego, A. Mallet, M. Lany, G. Santi, B. Revaz, J. Cortés, *et al.*, "A truly-redundant aerial manipulator system with application to push-and-slide inspection in industrial plants," *IEEE Robotics and Automation Letters*, vol. 4, no. 2, pp. 1846–1851, 2019.

[16] A. Suarez, P. R. Soria, G. Heredia, B. C. Arrue, and A. Ollero, "Anthropomorphic, compliant and lightweight dual arm system for aerial manipulation," in *2017 IEEE/RSJ International Conference on Intelligent Robots and Systems (IROS)*. IEEE, 2017, pp. 992–997.

[17] F. Ruggiero, M. A. Trujillo, R. Cano, H. Ascorbe, A. Viguria, C. Peréz, V. Lippiello, A. Ollero, and B. Siciliano, "A multilayer control for multirotor uavs equipped with a servo robot arm," in *2015 IEEE international conference on robotics and automation (ICRA)*. IEEE, 2015, pp. 4014–4020.

[18] D. Lee, H. Seo, D. Kim, and H. J. Kim, "Aerial manipulation using model predictive control for opening a hinged door," in *2020 IEEE International Conference on Robotics and Automation (ICRA)*. IEEE, 2020, pp. 1237–1242.

[19] A. Yiğit, G. Grappe, L. Cuvillon, S. Durand, and J. Gangloff, "Preliminary study of an aerial manipulator with elastic suspension," in *2020 IEEE International Conference on Robotics and Automation (ICRA)*. IEEE, 2020, pp. 4287–4293.

[20] S. Hamaza, I. Georgilas, G. Heredia, A. Ollero, and T. Richardson, "Design, modeling, and control of an aerial manipulator for placement and retrieval of sensors in the environment," *Journal of Field Robotics*, vol. 37, no. 7, pp. 1224–1245, 2020.